Electrochimica Acta 246 (2017) 280–284

Contents lists available at ScienceDirect

Electrochimica Acta

journal homepage: www.elsevier.com/locate/electacta

Research paper

$LaSn_3$ as a novel anode material for Na-ion battery

Hiroyuki Usui[a,b], Yasuhiro Domi[a,b], Sachi Ohshima[a,b], Hiroki Sakaguchi[a,b,*]

[a] Department of Chemistry and Biotechnology, Graduate School of Engineering, Tottori University, 4-101 Minami, Koyama-cho, Tottori 680-8552, Japan
[b] Center for Research on Green Sustainable Chemistry, Tottori University, 4-101 Minami, Koyama-cho, Tottori 680-8552, Japan

ARTICLE INFO

Article history:
Received 17 March 2017
Received in revised form 2 May 2017
Accepted 12 May 2017
Available online 10 June 2017

Keywords:
Lanthanum stannide
Samarium stannide
Na-ion battery
Anode material
Thick-film electrode

ABSTRACT

As a novel Na-ion battery anode, we studied electrochemical reactions of a $LaSn_3$ electrode, and evaluated its cycling performance by comparison with that of a $SmSn_3$ electrode. The $LaSn_3$ electrode showed a reversible capacity of 580 mA h cm^{-3} at the first cycle, and a gradual increase in the capacity with cycling number. The $LaSn_3$ electrode exhibited a high capacity of 1470 mA h cm^{-3} even at the 400th cycle, which is three times higher than that of a hard carbon electrode. The electrode reactions of elemental Sn were observed in a cyclic voltammetry profile of the $LaSn_3$ electrode, indicating that a phase separation of $LaSn_3$ gradually occurs to form Sn. We suggested that the phase separation provides a Na-inactive La_3Sn_5 matrix, which can suppress the aggregation of Sn particles and can improve the cyclability. On the other hand, the $SmSn_3$ electrode showed a higher initial capacity of 970 mA h cm^{-3} and an earlier capacity decay by the 200th cycle. It is suggested that the phase separation of $SmSn_3$ progresses more rapidly while that of $LaSn_3$ slowly occurs because of a higher thermodynamic stability for $LaSn_3$ than $SmSn_3$.

1. Introduction

The use of renewable energy resources such as solar radiation, wind, and waves has intensively received attention because of the rapid exhaustion of fossil fuel resources and the resulting increase in environmental pollutions. In order to effectively utilize these renewable resources, we need a large-scale stationary battery system. Li-ion battery (LIB) and Na-ion battery (NIB) are similar energy storage devices in the view point of their charge–discharge mechanisms in which alkali metal ions can be inserted into active materials of anode and cathode in the batteries. Taking the natural abundance, the geometrical availability, and the cost into consideration, Na resource is much favorable compared with Li resource for a large-scale production of stationary battery.

As anode materials of NIB, researchers have been investigated hard carbons with a nanopore structure enabling reversible Na-insertion/extraction [1–3]. They have reported that the hard carbon electrodes exhibited stable cyclabilities and reversible capacities of 220–260 mA h g^{-1} for 100 charge–discharge cycles. The performances are very good. A drawback of hard carbon is, however, its low specific density less than 1.5 g cm^{-3}. For the stationary battery application, the important issue is specific capacity per unit volume rather than that per unit weight. The hard carbon with such low specific density has an essential disadvantage in terms of capacity per unit volume. For this issue, the authors have focused tin (Sn) with a high theoretical capacity of 847 mA h g^{-1} and a high specific density of 7.37 g cm^{-3}, and have developed new anodes materials based on Sn [4,5]. An aggregation of Sn, however, occurs by charge–discharge reactions, resulting in an electrical isolation of active material layer and a rapid capacity decay [4,5]. Rare earth elements can alloy with Sn to form binary alloy phases with high specific densities. Lanthanum (La) is relatively available and one of the less expensive metals among rare earth elements. $LaSn_3$ is the most Sn-rich phase in the La–Sn alloys, and has high specific density of 7.57 g cm^{-3}. Thus, in this study, we investigated for the first time anode properties of $LaSn_3$ electrode as a new NIB anode material. In addition, we selected samarium (Sm) as another rare earth element, and prepared electrode consisting of studied $SmSn_3$ with specific density of 7.84 g cm^{-3}. The difference in the anode performances was investigated for the $LaSn_3$ anode and the $SmSn_3$ anode.

2. Experimental

An active material powder of $LaSn_3$ was synthesized by a mechanical alloying (MA) method in Ar gas atmosphere. Elemental La chips and Sn powder were put in a stainless steel vessel together with stainless steel balls so that the weight ratio of La:Sn was 1:3. The MA was performed using a high-energy planetary ball mill (P-6, Fritsch) for 20 hours with a rotation speed of 300 rpm at room

* Corresponding author.
E-mail address: sakaguch@chem.tottori-u.ac.jp (H. Sakaguchi).

http://dx.doi.org/10.1016/j.electacta.2017.05.071
0013-4686/

temperature. The crystal structure of the powder obtained was confirmed by using X-ray diffraction (XRD, Ultima IV, Rigaku) to be identified as a cubic $AuCu_3$ type structure (Inorganic Crystal Structure Database, ICSD No.01-071-9456) as shown in Fig.S1. For comparison, an active material powder of $SmSn_3$ was also synthesized by the MA for 10 h (Fig.S2). The surface morphologies of the powders were observed by a field emission scanning electron microscope (FE-SEM, JSM-6701F, JEOL Ltd.). The crystallite sizes and the particle sizes were estimated from the XRD results and the SEM images (Fig.S3), respectively. No significant difference was observed for these sizes between the $LaSn_3$ and $SmSn_3$ powders.

Thick-film electrodes of $LaSn_3$ and $SmSn_3$ were prepared by a gas-deposition (GD) method [6,7]. Unlike conventional slurry-based electrodes, any binder or conductive material are not required for the GD method. In the process of film preparation, active material particles are accelerated to high speeds of about 150–500 m s^{-1} by a carrier gas ejected from a gas nozzle. A strong adhesion of the particles results from a high impact energy of collision between the particles and substrates. An active material layer can be made only of the particles, which is a remarkable advantage to evaluate the fundamental electrode reactions because no side reaction occurs for binder and conductive material. In this study, the GD was performed under conditions with a nozzle diameter of 0.8 mm, a Cu current collector of thickness 20 μm, a Ar carrier gas differential pressure of 7.0×10^5 Pa, and a nozzle–substrate distance of 10 mm. The weights of the active material layers were within the range of 70–80 μg. The thickness of the active material layers were 2–4 μm. The Sn electrode has a smooth surface because of Sn's high ductility, while the $LaSn_3$ electrode showed a relatively rough surface (Fig.S4).

To evaluate NIB anode performances, we assembled 2032-type coin cells consisting of the $LaSn_3$ and $SmSn_3$ electrodes as the working electrode, Na foil counter electrode, electrolyte, and glass fiber separator. We used an ionic liquid electrolyte because conventional organic electrolyte was not applicable to these electrodes (Fig.S5) owing to its reductive decomposition during charge−discharge reactions. The ionic liquid electrolyte used was sodium bis(fluorosulfonyl)amide (NaFSA)-dissolved *N*-methyl-*N*-propylpyrrolidinium bis(fluorosulfonyl)amide (Py13-FSA) with a concentration of 1 mol dm^{-3}. The authors have recently demonstrated that this ionic liquid electrolyte can remarkably improve NIB anode properties of Sn-based electrodes because of its superior electrochemical stability [8]. Constant current charge–discharge tests were performed using an electrochemical measurement system (HJ-1001 SM8A, Hokuto Denko Co., Ltd.) in the potential range between 0.005 and 2.0 V vs. Na^+/Na at 303 K at the constant current density of 50 mA g^{-1}. The current density corresponds to *C*-rates of 0.082*C* for $LaSn_3$ and 0.084*C* for $SmSn_3$ when the theoretical capacities of $LaSn_3$ and $SmSn_3$ are 609 and 595 mA h g^{-1}. A cyclic voltammetry (CV) was carried out for the $LaSn_3$ electrode and an Sn electrode under a sweep rate of 0.1 mV s^{-1}. The active material synthesis, the gas-deposition, and the cell assembly were performed throughout in a purge-type glove box (Miwa MFG, DBO-2.5LNKPTS) filled with an Ar atmosphere in which O_2 concentration was below 1 ppm and dew point was below −100 °C (corresponding to H_2O concentration of 0.01 ppm).

To discuss the difference in the thermodynamic stabilities of $LaSn_3$ and $SmSn_3$, a first-principles calculation based on density functional theory (DFT) was performed using the projector augmented wave (PAW) method as implemented in the plane wave code of the Vienna Ab initio Simulation Package (VASP) [9]. A generalized gradient approximation (GGA) was used as the term exchange correlation with a kinetic energy cutoff of 350 eV. Brillouin zone sampling was performed with a $8 \times 8 \times 8$ *k* point mesh within a Gamma point centered mesh scheme. The crystal structures for calculation is shown in Fig. S6. The figures of the crystal structures were created using VESTA package by K. Momma and F. Izumi [10]. The formation energy of $LaSn_3$, $E_f(LaSn_3)$,was calculated by total energies E_{total} of $LaSn_3$, La, and Sn according to the following equation:

$$E_f(LaSn_3) = E_{total}(LaSn_3) - \{E_{total}(La) + 3E_{total}(Sn)\}.$$

3. Results and discussion

Fig. 1 shows charge–discharge curves of $LaSn_3$ electrode and $SmSn_3$ electrode at the 1st, 2nd and 100th cycles. For comparison, an initial charge−discharge curve of Sn electrode is also shown. The potential slopes from 0.9 to 0.5 V vs. Na^+/Na were observed in the charge (sodiation) processes of $LaSn_3$, $SmSn_3$, and Sn electrodes, which is attributed to the reductive decomposition of the ionic liquid electrolyte [11]. Obrovac et al. have previously revealed that a Sn electrode showed four potential plateaus originating from phase transformation between Sn, $NaSn_3$, NaSn, Na_9Sn_4, and $Na_{15}Sn_4$: the charge (sodiation) plateaus appeared at around 0.43, 0.20, 0.08, and 0.05 V vs. Na^+/Na, while the discharge (desodiation) plateaus appeared at around 0.14, 0.23, 0.55, and 0.65 V vs. Na^+/Na [12,13]. Jung et al. have also reported a similar result: the charge plateaus were observed at 0.45, 0.18, 0.08, and 0.04 V vs. Na^+/Na, and the discharge plateaus were found at 0.14, 0.25, 0.53, and

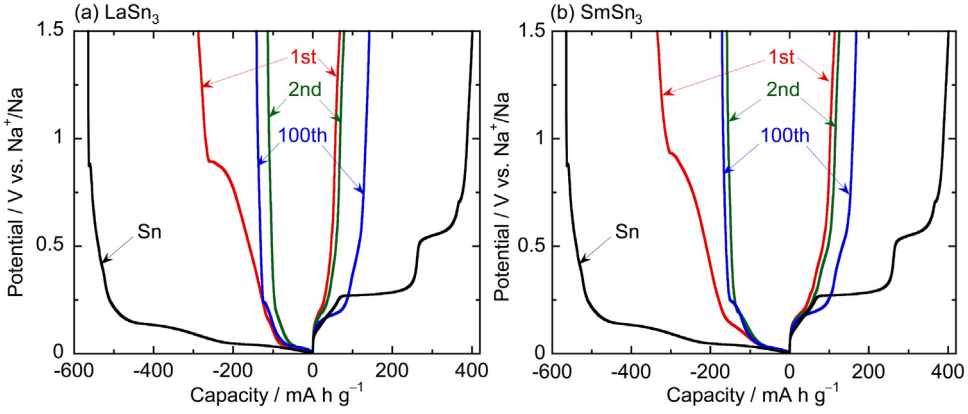

Fig. 1. Charge–discharge curves of (a) $LaSn_3$ electrode and (b) $SmSn_3$ electrode in ionic liquid electrolyte (NaFSA/Py13-FSA). For comparison, the initial charge−discharge curve of Sn electrode was also shown in the figures.